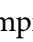




Optogenetic confirmation of transverse-tubular membrane excitability in intact cardiac myocytes

Marina Scardigli¹, Michal Pásek^{2,3}, Lorenzo Santini⁴, Chiara Palandri⁴, Emilia Conti^{5,6}, Claudia Crocini^{7,8}, Marina Campione⁹, Leslie M. Loew¹⁰ , Antoine A. F. de Vries¹¹, Daniël A. Pijnappels¹¹, Francesco S. Pavone⁵, Corrado Poggesi¹, Elisabetta Cerbai^{4,5}, Raffaele Coppini⁴, Peter Kohl¹² , Cecilia Ferrantini¹ and Leonardo Sacconi^{5,12,13} 

¹Department of Experimental and Clinical Medicine, University of Florence, Florence, Italy

²Institute of Thermomechanics, Czech Academy of Science, Prague, Czech Republic

³Department of Physiology, Faculty of Medicine, Masaryk University, Brno, Czech Republic

⁴Department of Neurology, Psychology, Drug Sciences and Child Health, University of Florence, Florence, Italy

⁵European Laboratory for Non-Linear Spectroscopy – LENS, Sesto Fiorentino, Italy

⁶Neuroscience Institute, National Research Council, Pisa, Italy

⁷DZHK (German Centre for Cardiovascular Research), Partner Site Berlin, Berlin, Germany

⁸Max Rubner Center for Cardiovascular Metabolic Renal Research (MRC), Deutsches Herzzentrum der Charité (DHZC), Charité-Universitätsmedizin Berlin, Berlin, Germany

⁹Institute of Neuroscience (IN-CNR) and Department of Biomedical Science, University of Padua, Padua, Italy

¹⁰Center for Cell Analysis and Modeling, University of Connecticut, Farmington, CT, USA

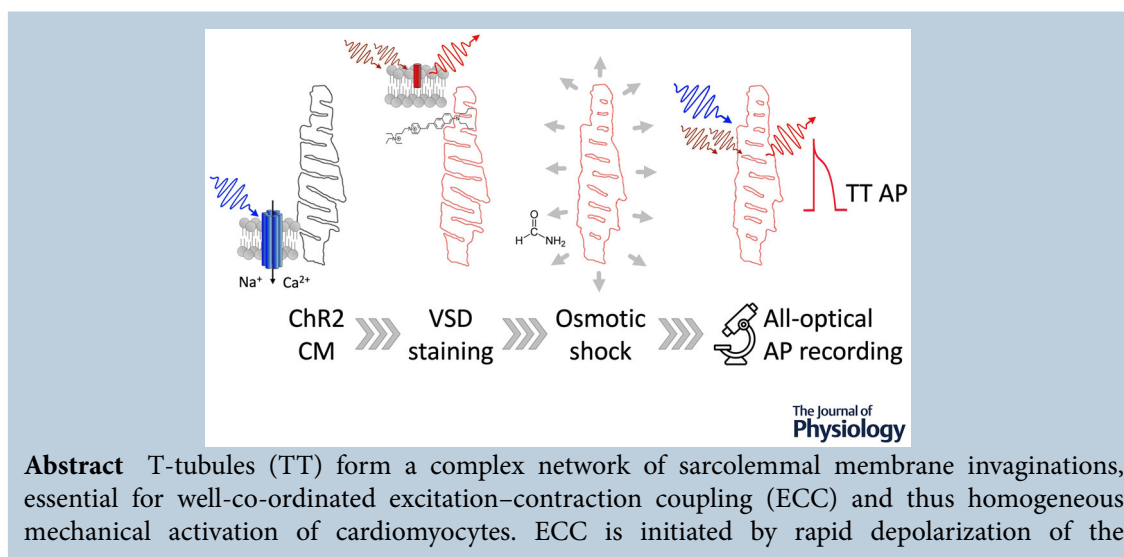
¹¹Laboratory of Experimental Cardiology, Department of Cardiology, Leiden University Medical Center, Leiden, The Netherlands

¹²Institute for Experimental Cardiovascular Medicine, University Heart Center and Medical Faculty, University of Freiburg, Freiburg, Germany

¹³Institute of Clinical Physiology, National Research Council (IFC-CNR), Florence, Italy

Handling Editors: Natalia Trayanova & Wolfgang Linke

The peer review history is available in the Supporting Information section of this article (<https://doi.org/10.1113/JP285202#support-information-section>).



M. Scardigli and M. Pásek contributed equally to this work.

C. Ferrantini and L. Sacconi contributed equally to this work.

This article was first published as a preprint. Scardigli M, Pásek M, Santini L, Palandri C, Conti E, Crocini C, Campione M, Loew L, deVries AAF, Pijnappels DA, Pavone FS, Poggesi C, Cerbai E, Coppini R, Kohl P, Ferrantini C, Sacconi L. 2023. Optogenetic confirmation of transverse-tubular membrane excitability in intact cardiac myocytes. bioRxiv. <https://doi.org/10.1101/2023.11.29.569144>

sarcolemmal membrane. Whether TT membrane depolarization is active (local generation of action potentials; AP) or passive (following depolarization of the outer cell surface sarcolemma; SS) has not been experimentally validated in cardiomyocytes. Based on the assessment of ion flux pathways needed for AP generation, we hypothesize that TT are excitable. We therefore explored TT excitability experimentally, using an all-optical approach to stimulate and record trans-membrane potential changes in TT that were structurally disconnected, and hence electrically insulated, from the SS membrane by transient osmotic shock. Our results establish that cardiomyocyte TT can generate AP. These AP show electrical features that differ substantially from those observed in SS, consistent with differences in the density of ion channels and transporters in the two different membrane domains. We propose that TT-generated AP represent a safety mechanism for TT AP propagation and ECC, which may be particularly relevant in pathophysiological settings where morpho-functional changes reduce the electrical connectivity between SS and TT membranes.

(Received 26 June 2023; accepted after revision 17 January 2024; first published online 13 February 2024)

Corresponding author L. Sacconi: Institute for Experimental Cardiovascular Medicine, University Heart Center and Medical Faculty, Elsassstr. 2Q, 79110 Freiburg, Germany. Email: leonardo.sacconi@uniklinik-freiburg.de

Abstract figure legend Methodological framework employed to dissect the electrical properties of isolated t-tubules (TT). Isolated cardiomyocytes with specific expression of Chr2 (Chr2 CM) are initially stained with a voltage-sensitive dye (VSD) suitable for two-photon imaging, thus allowing TT labelling and imaging. Subsequently, TTs are disconnected from the superficial sarcolemma using a formamide-based osmotic shock, and the electrical activity of isolated TTs is probed using a random-access two-photon microscope during optogenetic stimulation. This approach allowed the first recording of self-generated T-tubular action potentials (TT AP) in cardiac cells.

Key points

- Cardiomyocytes are characterized by a complex network of membrane invaginations (the T-tubular system) that propagate action potentials to the core of the cell, causing uniform excitation–contraction coupling across the cell.
- In the present study, we investigated whether the T-tubular system is able to generate action potentials autonomously, rather than following depolarization of the outer cell surface sarcolemma.
- For this purpose, we developed a fully optical platform to probe and manipulate the electrical dynamics of subcellular membrane domains.
- Our findings demonstrate that T-tubules are intrinsically excitable, revealing distinct characteristics of self-generated T-tubular action potentials.
- This active electrical capability would protect cells from voltage drops potentially occurring within the T-tubular network.

Introduction

Mammalian cardiomyocytes contain a complex transverse/axial network of sarcolemmal membrane invaginations, referred to henceforth as the T-tubular

(TT) system. In healthy cardiomyocytes, TT membranes are continuous with the surface sarcolemma (SS). SS and TT jointly mediate co-ordinated electrical and mechanical activation of individual cardiomyocytes

Marina Scardigli graduated in biotechnology at the University of Florence in 2014 and obtained her PhD at University of Siena in 2018, investigating the electrical properties of the cardiac T-tubular system. She worked as a postdoc at the European Laboratory for Non-Linear Spectroscopy in Italy, focusing her research on cardiac electrophysiology and on human brain structure using advanced optical imaging techniques. She is now part of the permanent research staff at the Department of Clinical and Experimental Medicine, University of Florence, working on biophysics and muscle mechanics in pathophysiological conditions.



(Tidball et al., 1991) by supporting excitation–contraction coupling (ECC) across the entire cell (Bers, 2002; Franzini-Armstrong et al., 1973).

Despite indications of non-homogeneous distribution of ion flux pathways and chemical gradients in SS and TT compartments, there are no significant differences between action potential (AP) profiles recorded in SS and TT membranes of healthy cardiomyocytes, presumably because the two membrane compartments are electrically well-coupled (Sacconi et al., 2012). The characteristic length constant of electrotonic potential decay in TT is one order of magnitude larger than a typical cardiomyocyte radius (Scardigli et al., 2017), indicating a remarkable safety factor for co-ordinated voltage changes across the entire sarcolemma in healthy cardiomyocytes. This may be impaired, however, in cardiac diseases where substantial TT remodelling has been observed (Crocini et al., 2014; Sacconi et al., 2012).

This poses an interesting and as yet experimentally unresolved question: is TT membrane depolarization, and hence well-co-ordinated initiation of ECC across the entire cell volume, dependent on active AP generation in TT, or is it driven by passive electrotonic effects from AP generation in the SS membrane?

We therefore implemented an experimental investigation which involved, first, electrical insulation of TT from SS membranes and, second, an all-optical approach to locally depolarize TT or SS membranes at the same time as tracking changes in their trans-membrane potentials. Electrical insulation of TT from SS membranes was achieved by transient exposure of cells to an acute osmotic shock (Ferrantini et al., 2014; Kawai et al., 1999), which ties off TT near their junctions with the SS membrane. Using random-access multiphoton (RAMP) microscopy and cardiomyocytes containing a combination of either CheRiff or ChR2 (optogenetic actuators) (Hochbaum et al., 2014) and di-4-AN(F)EPPTEA (voltage-sensitive dye; VSD) (Yan et al., 2012), we found that TT membranes are electrically excitable (i.e. able to generate local AP even after electrical insulation from the SS).

Methods

Animals

We used 12-week-old female transgenic mice (ChR2-mhc6-cre +) with cardiomyocyte-specific expression of ChR2 (H134R variant) and age-matched mice from the same strain (C57BL/6J). Animal handling and procedures were performed in accordance with guidelines in Directive 2010/63/EU of the European Parliament (protection of animals used for scientific purposes). The experimental protocol was approved by the Italian Ministry of Health (authorization number 944/2018-PR).

Adeno-associated virus-based gene transfer of CheRiff

Mouse hearts were driven to express the optogenetic actuator CheRiff (Hochbaum et al., 2014) coupled with enhanced green fluorescent protein (eGFP) by adeno-associated virus (AAV) based transduction using AAV2/9.45.GgTnnt2.CheRiff~eGFP.WHVPRE.SV40pA particles. This AAV (Pulicherla et al., 2011) contains a transgene consisting of the chicken cardiac troponin T promoter, the coding sequence of the blue light-activatable cationic channelrhodopsin CheRiff tagged at its C terminus with eGFP, the woodchuck hepatitis virus post-transcriptional regulatory element and the simian virus 40 polyadenylation signal. Production, purification and quantification of these vector particles was carried out as described in Nyns et al. (2017). Systemic delivery of AAV particles was performed as described in Yan et al. (2012). Briefly, AAV particles were injected into the left jugular vein of mice anaesthetized with isoflurane (3% for induction and 1.5% for maintenance, in oxygen). Body temperature was maintained at 37°C using a homeothermic blanket system (#50300; Stoelting Co., Wood Dale, IL, USA) and mice were monitored using respiratory rate and toe pinch response tests throughout the procedure. Mice were placed on a stereotaxic apparatus and shaved over the chest to allow identification of the jugular vein underneath the mouse skin, after which the shaved area was sterilized with betadine and 70% ethanol. Next, lidocaine solution was applied to the skin surface and a 5 mm long cervical incision was made to expose the jugular vein. An insulin syringe (30G × 1/6"; Biotekne, Casalecchio di Reno, Italy) was used to slowly inject 200 μL of the injection mix composed of $\sim 2 \times 10^{11}$ genome copies of AAV diluted in phosphate-buffered saline (P4417; Merck, Rahway, NJ, USA) containing 2.5 mM MgCl₂ and 1 mM KCl. After stopping of the bleeding with surgical swabs, the skin was sutured with Vicryl Plus Ethicon (VCP394H; Johnson & Johnson Medical NV, Maelen, Belgium) and mice were placed back into their cages. Tail vein injection was also explored. To this end, tails were cleaned and sterilized with 70% ethanol and a bent needle of an insulin syringe was inserted into one of the lateral veins, followed by the slow administration of the same injection mix. At 4 weeks post-transduction, hearts were excised and used for the isolation of ventricular cardiomyocytes as described below.

Cardiomyocyte isolation

Left ventricular cardiomyocytes from all experimental groups were isolated by enzymatic dissociation, as previously described (Crocini et al., 2016). In brief, animals were heparinized (5000 U kg⁻¹ body weight, i.p.) and deeply anaesthetized with isoflurane. The heart was

excised and the ascending aorta was cannulated for perfusion in Langendorff mode. Cell isolation solution was calcium-free and contained (in mM): 113 NaCl, 4.7 KCl, 0.6 KH_2PO_4 , 0.6 Na_2HPO_4 , 1.2 MgSO_4 , 12 NaHCO_3 , 10 KHCO_3 , 10 HEPES, 30 taurine, 10 glucose and 10 2,3-butanedionemonoxime, pH 7.3, adjusted with NaOH). After perfusion for 3–4 min with a constant flow of 7–8 mL min^{-1} at 37°C, the cell isolation solution was switched to a recirculating enzyme-containing solution, made from the cell isolation solution by adding 0.1 mg mL^{-1} Liberase (Merck Life Science S.r.l., Darmstadt, Germany). After 7 min, the left ventricle was harvested, cut into small pieces in cell isolation solution supplemented with 1 mg mL^{-1} bovine serum albumin, and gently stirred to facilitate dissociation of cardiomyocytes. The cell suspension was allowed to settle at room temperature (RT, 20°C) for 10 min, before the cell pellet was re-suspended in a calcium-free, HEPES-buffered Tyrode's solution. HEPES-buffered Tyrode's solution contained (in mM): 133 NaCl, 4.8 KCl, 1.2 MgCl_2 , 10 glucose, 10 μM blebbistatin, 4 μM cytochalasin D and 10 HEPES, pH 7.35, adjusted with NaOH, unless otherwise specified. Isolated ventricular cardiomyocytes were gradually re-adapted at RT to calcium by adding 50 or 100 μM CaCl_2 every 5–8 min, until a concentration of 1 mM CaCl_2 was reached.

Sarcolemma labelling

Cells were placed in HEPES-buffered Tyrode's solution containing 0.5 mM CaCl_2 . Cardiomyocyte staining was performed by adding 2 $\mu\text{g mL}^{-1}$ of the VSD (Yan et al., 2012) (from 2 mg mL^{-1} stock, dissolved in ethanol). After 5 min, cells were resuspended in fresh HEPES-buffered Tyrode's solution containing 1 mM CaCl_2 . Staining and imaging were performed at RT.

Acute detubulation

Disconnection of TT membranes from the SS (henceforth called 'detubulation'; DETUB) was achieved by hyper-osmotic shock, as previously described (Ferrantini et al., 2014; Kawai et al., 1999). Briefly, 1.5 M formamide was added to the cell suspension (in HEPES-buffered Tyrode's solution containing 0.5 mM CaCl_2). After 15 min, cells were resuspended rapidly in fresh HEPES-buffered Tyrode's solution containing 1 mM CaCl_2 . The detubulation procedure was performed at RT. For RAMP measurements detubulation was induced after sarcolemmal staining with VSD.

Quantification of T-tubular density

Isolated cardiomyocytes, both intact (CTRL) and formamide-treated (DETUB) were incubated for

20 min with 5 μM of Di-3-ANEPPDHQ (Thermo Fisher Scientific, Waltham, MA, USA) membrane dye. This approach allowed us to investigate the fraction of detached T-tubules because only those still connected with the surface were labelled. CTRL and DETUB cells were resuspended in calcium-free HEPES-buffered Tyrode's solution, placed into a glass-bottomed chamber (P50G-0-14-F; MatTek, Ashland, MA, USA) and observed using a 63 \times oil immersion objective on a TCS5 confocal microscope (Leica, Wetzlar, Germany). The excitation wavelength was 488 nm and the detection window was set to 504–649 nm. TT quantitative analysis was performed using AutoTT (Guo & Song, 2014) on confocal images, as previously described (Crocini et al., 2016). In brief, AutoTT skeletonizes the global architecture of the TT system to extract morphological patterns, discriminating transverse and axial elements of the system. To determine the densities of transverse and axial elements, the total number of pixels in each of these TT subcategories was divided by the total number of pixels of the intracellular region imaged.

Patch clamp experiments

To perform patch clamp recordings, viable ventricular cardiomyocytes were resuspended with HEPES-buffered Tyrode's solution containing 1.8 mM CaCl_2 at RT. Patch clamp data recording and analysis were performed using a Multiclamp700B amplifier in conjunction with pClamp10.0 and a DigiData 1440A AD/DA interface (Molecular Devices, San Jose, CA, USA). AP recordings and K^+ current measurements were conducted in whole-cell ruptured patch mode. The pipette solution contained (in mM): 130 K-aspartate, 0.1 Na-GTP, 5 $\text{Na}_2\text{-ATP}$, 11 EGTA, 5 CaCl_2 , 2 MgCl_2 and 10 HEPES, pH 7.2 adjusted with KOH; free $[\text{Ca}^{2+}]$ was calculated using maxchelator (<https://somapp.ucdmc.ucdavis.edu/pharmacology/bers/maxchelator/>) and was equal to 243 nM. For K^+ current measurements, 0.3 mM CdCl_2 was added to the bath solution. AP trains were electrically elicited with short depolarizing stimuli (3 ms square current pulses, 500–1000 pA) at 1 Hz pacing rate. Recordings of global potassium current (I_{K}) were carried out using depolarization steps of 900 ms, from -50 mV to 0 mV, immediately after eliciting the Na current. $I_{\text{K-peak}}$ was calculated as the maximum current, whereas $I_{\text{K-end}}$ is the residual outward current at 900 ms. For L-type calcium (I_{CaL}) and sodium (I_{Na}) current recordings, the pipette solution contained (in mM) 120 CsCl, 10 HEPES, 5 Na_2ATP , 10 TEACl, 5 MgCl_2 , 4.3 CaCl_2 and 10 EGTA (calculated free $[\text{Ca}^{2+}] = 226$ nM), pH 7.2, adjusted with CsOH, whereas the external solution contained (in mM) 135 NaCl, 5.4 CsCl, 10 glucose, 10 HEPES, 1 MgCl_2 , 1.8 CaCl_2 , 0.33 NaH_2PO_4 and 0.3 BaCl_2 , pH 7.4, adjusted with CsOH. Peak sodium current (I_{Na}) was elicited

with a 15 ms depolarizing step from -80 mV (holding potential) to -45 mV, whereas I_{CaL} was elicited with a longer (200 ms) depolarization step from -45 mV to 0 mV, immediately eliciting the Na current. I_{Na} and I_{CaL} were induced at a repeat rate of 1 Hz.

Modelling

The model used in the present study is based on a previously published model of rat ventricular cardiomyocytes incorporating TT (Pasek et al., 2006) and was modified to reproduce the key properties of the mouse ventricular cardiomyocytes (Bondarenko et al., 2004). Modifications included: (1) adjustment of geometric parameters of the model cell; (2) reformulation of ion flux pathways in SS and TT membranes; (3) adaptation of sarcoplasmic reticulum Ca^{2+} pump activity; and (4) adjustment of ion exchange between the TT lumen and the extracellular space. All modifications are described in detail in the appendix. The model was implemented in MATLAB, version 7.2 (MathWorks, Inc., Natick, MA, USA). Computation of the system of 47 non-linear differential equations was performed using the solver for stiff system ode15s (MATLAB). Model equations were solved simultaneously, using a variable time-step (0.4×10^{-6} – 0.1 s) adjusted to keep the estimated relative error of inner variables below a threshold value of 10^{-6} . Steady-state behaviour of the model was achieved by running it for 600 s of equivalent cell lifetime at the specified stimulation frequencies. The MATLAB code of the model is available at <https://www.it.cas.cz/en/d3/1033>.

RAMP microscope and optogenetics stimulation

The basic design of our RAMP microscope has been described elsewhere (Crocini et al., 2014; Sacconi et al., 2012; Scardigli et al., 2017). In the present study, the system was implemented with a fibre-based optical stimulation system for optogenetic pacing. A LED (M470F3; Thorlabs, Bergkirchen, Germany) operating at 470 ± 25 nm was employed as a fibre-coupled light source and a 3-D micromanipulator was used to place the distal end of the multimode optical fibre (FG200UEA; Thorlabs) in proximity of the cell. The numerical aperture (N.A.) of the optical fibre and the angle of the fibre with respect to the main optical axis were chosen to avoid direct collection of blue light by the RAMP excitation/detection objective ($40\times$, water immersion, N.A. 0.8; Olympus, Tokyo, Japan). This is crucial, given that blue light can generate unwanted phosphorescent signals inside the objective glass that may affect optical recordings (not shown). The RAMP fluorescence signal was detected using a photon-counting module, based on the GaAsP photomultiplier tube (PMT) with an ultra-fast gate circuit (H11706P-40; Hamamatsu, Shizuoka, Japan). An emission filter of 655 ± 20 nm

was used for fluorescence detection. A trigger distributor switched off the high-voltage power supply circuit of the PMT during optical stimulation. This avoids the possibility that endogenous or exogenous fluorescence signals overload the PMT during blue light illumination. Cells were optically paced using pulses of blue light with a duration of 3 ms and a light intensity of 10 mW mm^{-2} at the output of the optical fibre. Alternatively, cells could be electrically field-stimulated using two parallel platinum wires (diameter $250 \mu\text{m}$), placed in the bath at a distance of 6.3 mm. Square pulses of 10–20 V (swapping anode and cathode), lasting 3 ms, were used to trigger AP. In a typical RAMP measurement, we performed one line-scan along the SS, and two to four line-scans on different TT membrane segments. The length of scanned lines ranged from 5 to $10 \mu\text{m}$, with an integration time per membrane pass of $\sim 200 \mu\text{s}$, leading to a temporal resolution of 0.4–2 ms. Optical recordings in detubulated cells were performed within 30 min after the formamide treatment to limit a potential luminal ion concentrations variation of sealed-off TT. Opto-electronic components of the setup were computer-controlled with custom-made software developed in LabVIEW 7.1 (National Instruments, Austin, TX, USA). Optical recordings were analyzed with a custom-made software written in LabVIEW 2013 (National Instruments).

Statistical analysis

For each experimental condition, we assess whether measured data came from a normal, log-normal or other distribution, performing a Shapiro–Wilk test of all data before and after their logarithmic transformation. The median was used as the best representation of central data values. In patch clamp experiments, data from one cell were averaged, and this average was used for comparison and statistical analysis. One-way analysis of variance (ANOVA) tests were used to compare electrophysiological features between CTRL and DETUB. In optical recordings, two-way ANOVA tests were used to compare electrophysiological features between SS and TT at different stimulation modalities, the Bonferroni *post hoc* analysis was used. AP optical stimulation efficiency in CTRL and DETUB was compared using Fisher's exact test. Statistical analysis was performed using OriginPro 2018 (OriginLab, Northampton, MA, USA).

Results

Ion flux pathways across sarcolemma in mouse cardiomyocyte and *in silico* assessment of TT excitability

Structural and patch clamp data from ventricular cardiomyocytes which underwent acute detubulation through

osmotic shock (DETUB) were compared to intact cells (CTRL) to assess AP-relevant ion current distributions between TT and SS (Fig. 1). Our data indicate that L-type Ca^{2+} channels are expressed predominantly in the TT membrane (note: I_{CaL} density was reduced by ~ 0.5 in

DETUB, compared to CTRL cells), whereas Na^{+} and K^{+} channels densities appear to be uniform across the whole cell membrane. Consistent with the high I_{CaL} density in TT, a reduction of AP duration at 50% and 90% repolarization was found in DETUB cells, compared to

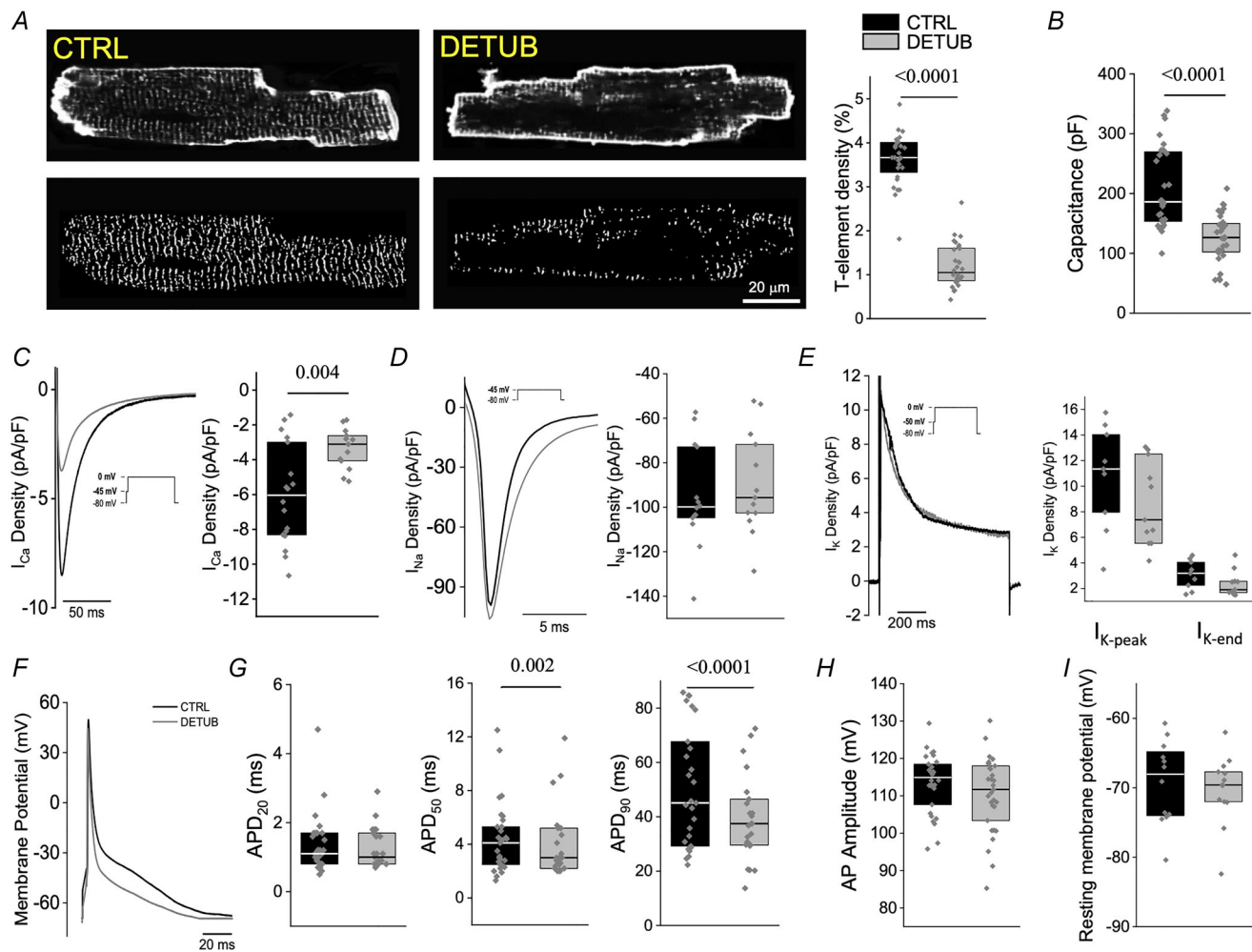


Figure 1. Patch clamp recordings on CTRL and DETUB cells

A, two representative confocal images of intact (CTRL) and detubulated (DETUB) cardiomyocytes. Sarcolemma stained with Di-3-ANEPPDHQ. Bottom: correspondent images of the same cells showing a skeletonized TT system, obtained with AUTO-TT. Right: TT density expressed as a percentage (%) in CTRL (black box; $N = 3$ animal, $n = 28$ cells) and DETUB (grey box; $N = 3$, $n = 32$) cardiomyocytes. B, cell capacitance (pF), measured by dividing membrane time constant by membrane resistance, recorded in CTRL ($N = 6$, $n = 30$) and DETUB ($N = 6$, $n = 31$) cardiomyocytes. C, representative traces and average values of L-Type Ca^{2+} current density (I_{CaL}) at 0 mV from CTRL ($N = 5$, $n = 18$) and DETUB ($N = 5$, $n = 13$) cardiomyocytes. D, representative traces and average values of peak Na^{+} current density ($I_{\text{Na-peak}}$) at 0 mV from CTRL ($N = 5$, $n = 14$) and DETUB ($N = 5$, $n = 13$). E, representative traces of outward K^{+} current density (I_{K}) and average values of peak outward K^{+} current density ($I_{\text{K-peak}}$) and residual outward K^{+} current density at 900 ms ($I_{\text{K-end}}$) at 0 mV from CTRL ($N = 5$, $n = 9$) and DETUB ($N = 5$, $n = 12$). F, representative AP recorded in CTRL and in DETUB cardiomyocytes, paced at 1 Hz. G, duration at 20%, 50% and 90% of repolarization from AP peak (APD_{20} , APD_{50} and APD_{90} , respectively) recorded in CTRL ($N = 6$, $n = 30$) and DETUB ($N = 6$, $n = 31$) cardiomyocytes, stimulated at 1 Hz. H, AP amplitude expressed as the difference between the resting membrane potential (RMP) and the maximum potential recorded, stimulated at 1 Hz. I, RMP. Single data are reported as grey points and box plots with a range of 25th to 75th percentile are superimposed. Median values are represented by the line in box plots. P values were calculated with one-way ANOVA and the Bonferroni test. N indicates the number of animals and n the number of cells in each data series. Raw data are available at: <https://doi.org/10.6084/m9.figshare.23742231>. [Colour figure can be viewed at [wileyonlinelibrary.com](https://onlinelibrary.wiley.com/terms-and-conditions)]

CTRL, whereas no significant differences in AP amplitude or resting membrane potential were detected between the groups.

Measured ion flux pathways were incorporated into an adapted computer model of mouse ventricular cardiomyocytes with two ECC domains: SS and TT (for a detailed description, see the Appendix). The model predicts that, based on available electrophysiological data, TT are excitable and AP duration of isolated TT is longer than in SS alone (Fig. 2A). Nevertheless, the model also showed that co-ordinated ECC could be ensured both with active AP generation, or with passive electrotonic conduction, in TT (Fig. 2B) and that it is not possible to distinguish between these two possible mechanisms, based on available spatially resolved data on ECC and contraction dynamics in cardiac myocytes.

Optical induction and recording of AP in SS and TT of CTRL cells

RAMP microscopy was combined with optogenetic stimulation, employing an ultra-fast gated detection system (Fig. 3A). The experimental approach was first validated in intact ventricular myocytes, constitutively expressing a light-gated ion channel (ChR2) and labelled

with VSD. RAMP rapidly scanned linear segments on SS and TT membranes during electrical field stimulation or whole-cell optical stimulation. Both stimulation modes allowed AP induction in SS and TT membranes of CTRL cells (Fig. 3B and C). As expected, electrically and optically stimulated AP amplitudes and kinetics in TT are not significantly different from those in SS (Fig. 3D–F).

Comparing AP features between the two stimulation modalities, we found a substantially longer time-to-peak AP (~5-fold, 15 ms instead of 3 ms; TTP in Fig. 3E) during optical compared to electrical stimulation, as previously reported (Bruegmann et al., 2010). Effects of ChR2 activation on AP repolarization (e.g. APD₅₀ in Fig. 3F) were less pronounced or absent. These results indicate that a full-optical approach can be used to quantitatively assess AP dynamics in different sarcolemmal domains.

Of note, AP amplitudes are lower than what was found in our previous investigation (~20%) (Crocini et al., 2016). This is not unexpected considering that, in the present mouse line (Zaglia et al., 2015), the 1064 nm light excites both the VSD and ChR2-conjugated td-Tomato fluorescent protein (Drobizhev et al., 2011). In a subset of experiments where cardiomyocytes from CTRL mice were transfected with light-activated channels fused with eGFP (not excited at 1064 nm), we found (Fig. 4) that the relative

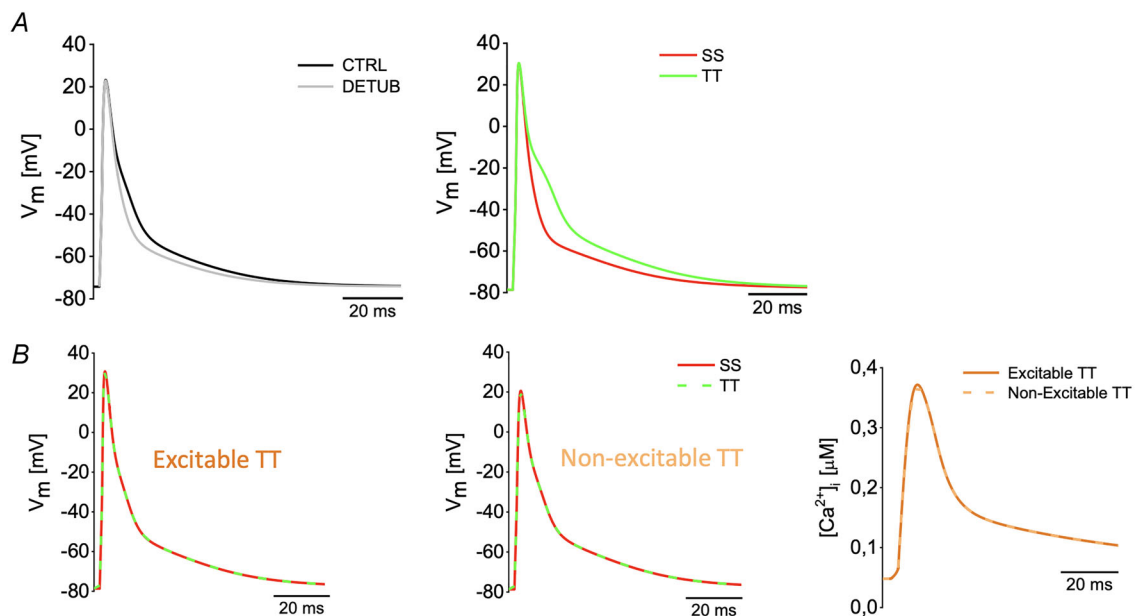


Figure 2. *In silico* prediction of TT membrane excitability

A, Left: simulation of 1 Hz steady-state AP shapes in CTRL (black) and DETUB cells (grey) assuming a residual TT fraction equal to zero. Intracellular ion concentrations were fixed at experimentally clamped values: $[Na^+]_i = 10$ mM, $[K^+]_i = 130$ mM and $[Ca^{2+}]_i = 200$ nM. Extracellular ion concentrations were: $[Na^+]_e = 140$ mM, $[K^+]_e = 5.4$ mM and $[Ca^{2+}]_e = 1.8$ mM. Right: simulation of TT (green trace) and SS (red trace) AP after separation of TT. TT lumen ion concentrations were close to the extracellular ion concentration: $[Na^+]_{TT} = 140$ mM, $[K^+]_{TT} = 5.4$ mM and $[Ca^{2+}]_{TT} = 1.8$ mM. B, simulated AP shapes in the presence (Excitable TT) and absence (Non-excitable TT) of the fast sodium current in TT (dashed green). Simulated cytosolic Ca^{2+} -transient in the presence of excitable TT (dark orange) and non-excitable TT (dashed light orange). Raw data are available at: <https://doi.org/10.6084/m9.figshare.23742231>. [Colour figure can be viewed at wileyonlinelibrary.com]

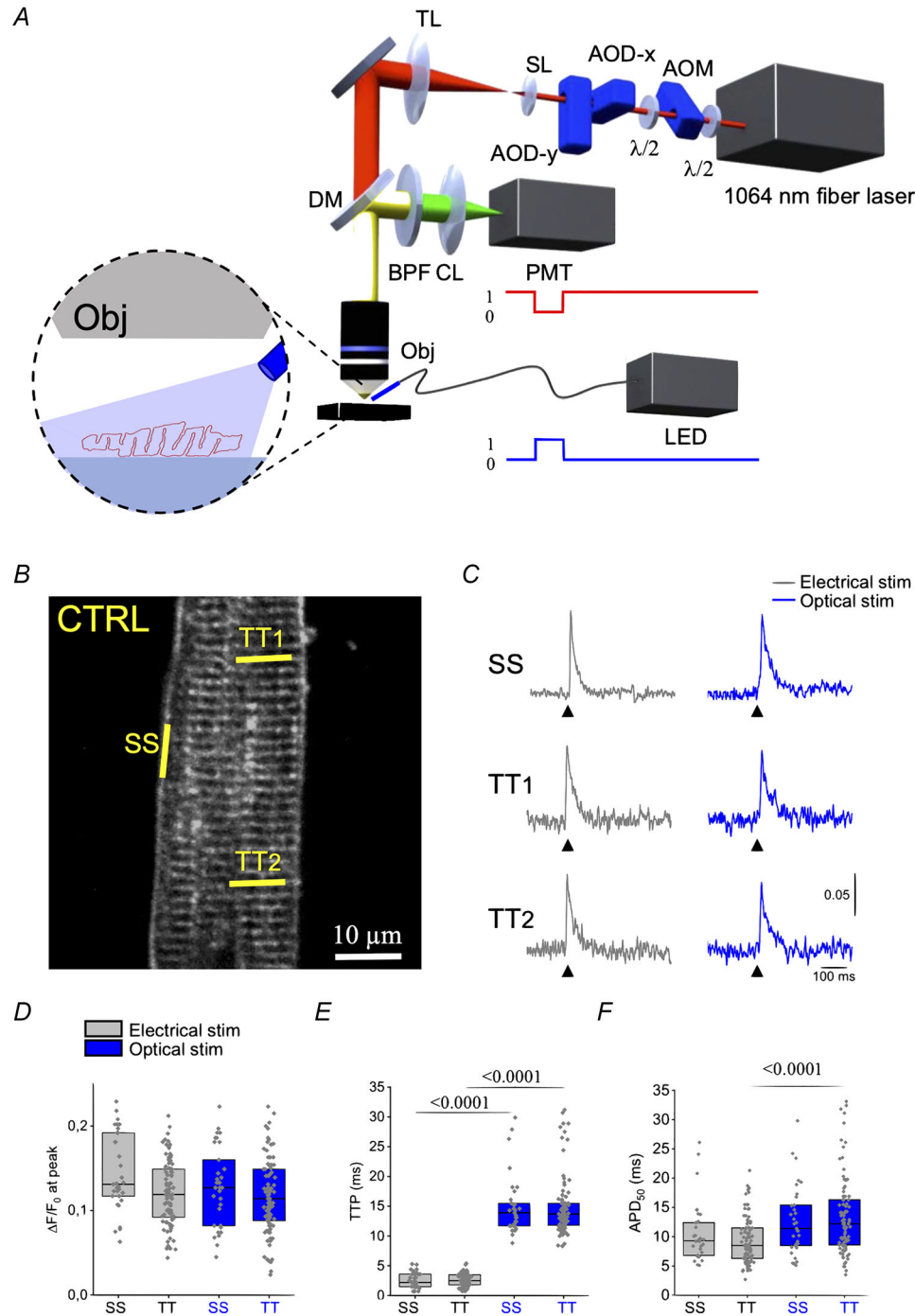


Figure 3. All-optical AP recording in TT and SS membrane sites of CTRL cardiomyocytes

A, scheme of the random access multiphoton (RAMP) microscope: 1064 nm fibre laser, an acousto-optic modulator (AOM), two orthogonally mounted acousto-optic deflectors (AOD-x and AOD-y), scanning lens (SL), tube lens (TL), dichroic mirror (DM), water immersion objective (Obj), band-pass filter (BPF), condenser lens (CL) and photo-multiplier tube (PMT). Cells were optically stimulated using a fibre-coupled LED, placing the distal end of the multimode optical fibre in the proximity of the cell (highlighted in the inset). A trigger distributor was used to switch-off the PMT (red traces) during optical stimulation (blue trace). **B**, two-photon fluorescence image of a ventricular myocyte constitutively expressing ChR2 and labelled with VSD. The yellow lines mark the probed membrane sites (SS, sarcolemma; TT₁ and TT₂, T-tubules). **C**, normalized fluorescence traces ($\Delta F/F_0$) recorded from the three scanned membrane domains (average of 10 sequential runs). An AP (elicited at 200 ms, black arrowheads) is clearly visible in all three sites, regardless of whether the cell was stimulated electrically or optically. AP elicited using electrical field are represented in grey, whereas APs evoked using optical stimulation are in blue. **D**, AP amplitude ($\Delta F/F_0$ at peak), **E** time-to-peak (TTP) and **F** APD₅₀, measured upon electrical (black)

or optical (blue) stimulation. Single cell data are reported as grey points and box plots with a range of 25th to 75th percentile are superimposed. Median values are represented by the line in box plots. Data from 33 SS and from 93 TT recordings ($N = 6$ animals, $n = 33$ cells). P values were calculated with two-way ANOVA and the Bonferroni test. Raw data are available at: <https://doi.org/10.6084/m9.figshare.23742231>. [Colour figure can be viewed at [wileyonlinelibrary.com](https://onlinelibrary.wiley.com)]

fluorescence change at the AP peak is restored to previously reported values, both upon electrical and optical stimulation.

Optical induction and recording of AP in SS and TT of DETUB cells

Next, we employed the same approach on Chr2-expressing cardiomyocytes that underwent acute detubulation. As indicated in Fig. 5A, cells were first stained with the VSD and then acutely detubulated by osmotic shock. Thereafter, AP were optically recorded from SS and TT membranes upon electrical or optical stimulation (ten pulses each) (Fig. 5B). As expected, upon electrical stimulation, TT that were detached from the SS did not exhibit AP (grey traces), showing no membrane voltage variation above the shot-noise (~ 5 mV). This means that structurally detached and electrically uncoupled TT are not excited by either the local extracellular field stimulation potential (which is Faraday-screened by the SS) or passively depolarized by AP elicited in SS membrane. Crucially, however, some of electrically disconnected (from the SS) TT can be triggered to generate AP using optical stimulation (AP+) (Fig. 5B, left). The amplitude distribution of optically induced AP in SS and TT is depicted in Fig. 5C. Although AP amplitude in SS can be described by an unimodal distribution, TT membrane potential exhibits

a pronounced bimodal profile, where most TT are silent (AP-) (Fig. 5B, right) but a fraction of TT (AP+) are intrinsically excitable. This bimodal distribution of AP amplitudes in TT suggests that AP require activation of voltage-dependent channels with threshold for activation (e.g. NaV1.5), rather than simply reflecting Chr2-induced inward currents. This is further confirmed in patch clamp experiments on single cardiomyocytes, where the effect of Chr2-induced photocurrents on the membrane potential was evaluated in the presence or absence of Na⁺ and Ca²⁺ channel blockers (Fig. 5D).

In keeping with *in silico* predictions, isolated TT that are able to generate AP (AP+) show slower repolarization compared to SS (increased AP duration at 50% repolarization), unravelling intrinsic features of TT-generated AP (Fig. 5E).

The fraction of TT that were optically excitable after osmotic detubulation (AP+) was only 10–15% of the structurally disconnected TT (Fig. 6A). We exclude the possibility that a low photo-current density would account for the lack of TT excitability in the majority of TT, based on the homogenous sarcolemmal distribution of Chr2 measured in this transgenic mouse model (Fig. 6B). However, a reduction of membrane excitability in sealed-off TT is not unexpected: luminal ion concentrations are no longer clamped to bulk extracellular levels, and this can affect the local electrochemical gradient and thus channel/transporter functionality.

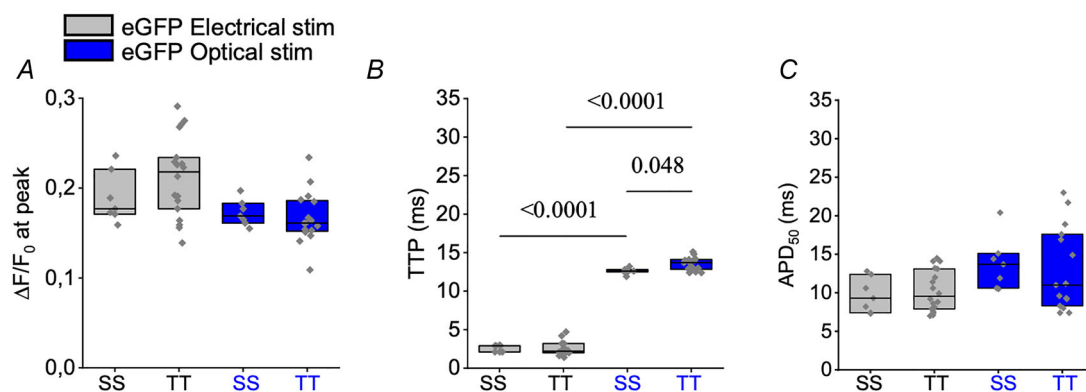


Figure 4. eGFP-Cheriff characterization

Columns showing (A) AP amplitudes ($\Delta F/F_0$ at peak), (B) time-to-peak (TTP) and (C) AP duration at 50% repolarization (APD_{50}) mean values measured in eGFP-Cheriff cells using electrical field stimulation (black) compared to optical stimulation (blue). Single cell data are reported as grey points and box plots with a range of 25th to 75th percentile are superimposed. Median values are represented by the line in box plots. Data from 7 SS and from 18 TT recordings ($N = 3$ animals, $n = 7$ cells). P values were calculated with two-way ANOVA and the Bonferroni test. Raw data are available at: <https://doi.org/10.6084/m9.figshare.23742231>. [Colour figure can be viewed at [wileyonlinelibrary.com](https://onlinelibrary.wiley.com)]

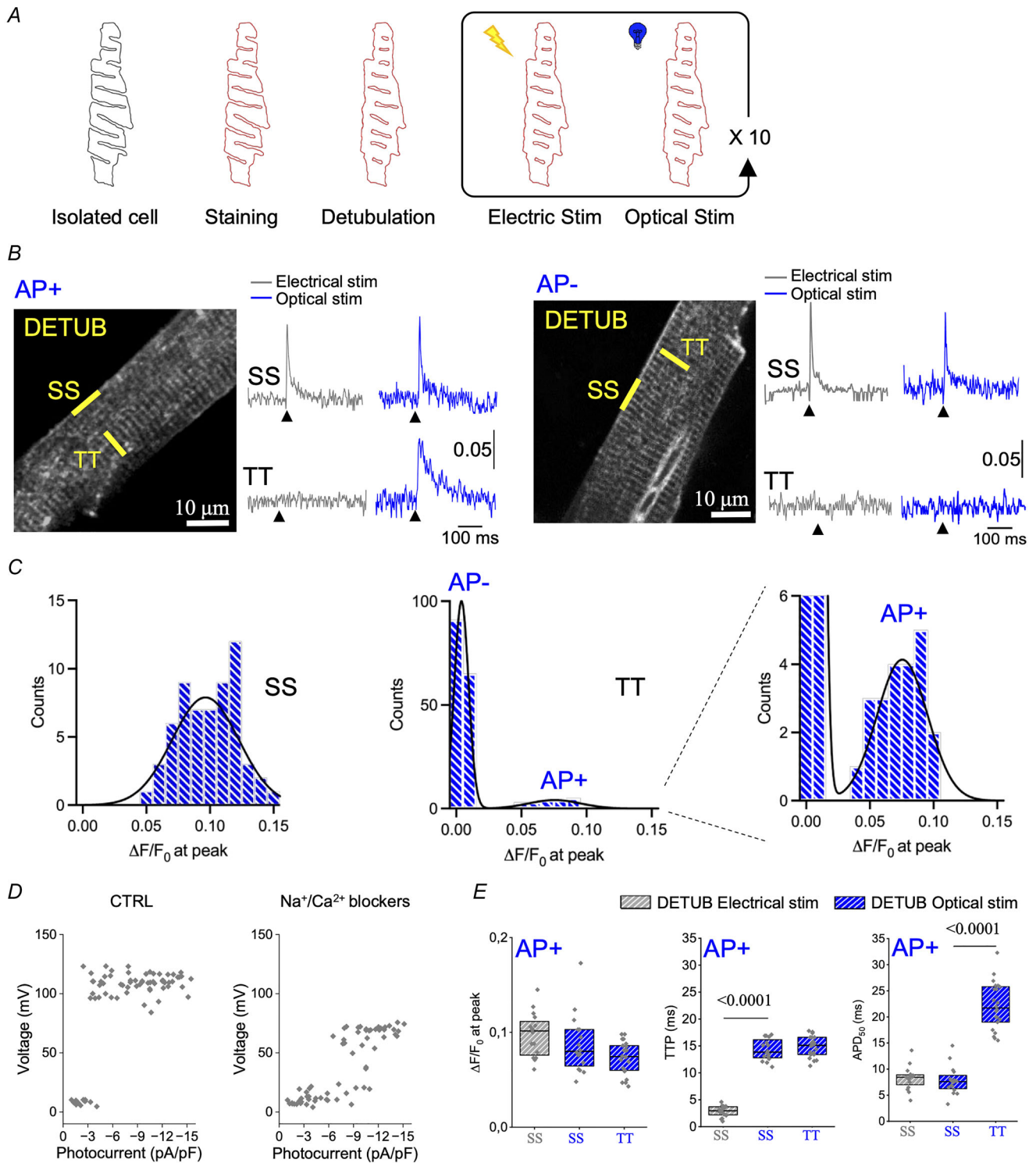


Figure 5. All-optical AP recording in TT and SS membrane sites of DETUB cardiomyocytes

A, representative scheme of DETUB, followed by electrical and optical AP stimulation. Isolated cardiomyocytes were stained using VSD (red), before acute detubulation. After DETUB, ten alternating cycles of electrical and optical stimulation were applied to elicit AP. B, two-photon fluorescence image of a DETUB ventricular myocyte constitutively expressing ChR2 and labelled with VSD. The yellow lines mark the probed membrane sites (SS, sarcolemma; TT, T-tubules). On the side of the images, normalized fluorescence traces ($\Delta F/F_0$) recorded from the two scanned sites (average of 10 sequential trials) in DETUB cells. During electrical stimulation, an AP (elicited at 200 ms, black arrowheads) is clearly visible in SS, whereas detached TT do not generate AP (grey traces). Using light (blue traces), it is possible to trigger AP in SS, whereas TT show one of two possible responses: an AP is

elicited in detached TT (left, AP+); or an AP is not triggered (right, AP-). C, distribution of AP amplitudes ($\Delta F/F_0$ at peak) in SS and TT. Right: zoom in of TT AP amplitudes to highlight the distribution of AP+. Data are from 68 SS and 178 TT ($N = 8$ animals, $n = 68$ cells). D, characterization of membrane potential variation vs. light-induced ChR2 photocurrent in CTRL cells in the absence and after treatment with TTX (at $30 \mu\text{M}$) and lacidipine ($10 \mu\text{M}$). Data from 19 cells ($N = 4$ animals). E, AP amplitude ($\Delta F/F_0$ at peak), time-to-peak (TTP) and APD₅₀, measured in DETUB cells upon electrical (grey) and optical (blue) stimulation. Single data are reported as grey points and box plots with a range of 25th to 75th percentile are superimposed. Median values are represented by the line in box plots. Data are from 16 SS and 22 TT. Two-way ANOVA and a Bonferroni test were applied. Raw data are available at: <https://doi.org/10.6084/m9.figshare.23742231>. [Colour figure can be viewed at [wileyonlinelibrary.com](https://onlinelibrary.wiley.com)]

Discussion

In the present study, we exploit the utility of light to probe crucial electrophysiological properties of SS and TT membranes in living cardiomyocytes. Our approach combines the advantages of RAMP microscopy, in terms of spatio-temporal resolution for local AP recording, with optogenetics for precise spatio-temporally controlled stimulation of subcellular membrane domains. Applying this methodology to cardiomyocytes where TT were structurally disconnected from the SS membrane by DETUB, we confirm that TT membranes are electrically excitable, such that they are able to generate AP, locally and independently from the SS. We further identify dissimilarities in AP shape between the two membrane domains that are in keeping with differences in their Ca^{2+} current density: AP duration at 50% repolarization is longer and AP-shape is more triangulated in TT than in SS.

We found that only a fraction (10–15%) of sealed-off TT is optically excitable. Although the full set of transporters and channels is present in the TT membrane of ventricular mouse cardiomyocytes (Berry et al., 2007; Bossuyt et al., 2009; Despa & Bers, 2007; Gadeberg et al., 2017a; Swift et al., 2007; Thomas et al., 2003), in the limited luminal volume of vacuolated TT, ion concentrations can fluctuate not only during cell activity, but also during periods of quiescence such as required to

implement the protocol for the present study (15–30 min). There are many reasons for which a sealed membrane compartment may lose excitability. Indeed, accumulation of K^+ and depletion of Ca^{2+} have been predicted and experimentally measured in sealed-off TT (Moench & Lopatin, 2014; Pasek et al., 2006). To illustrate this, ion fluctuations were phenomenologically introduced by increasing TT Na^+ background conductance in our *in silico* model. Figure 7 shows how a background Na^+ conductance may lead to time-dependent variations of TT ion concentrations and resting membrane potential. For example, if TT background Na^+ conductance is enhanced, TT resting potential depolarizes, so that the fraction of inactivated voltage-gated Na^+ channel increases, and TT excitability is disabled. In vacuolated TT, local luminal Na^+ concentration is continuously reset by the balance between passive Na^+ efflux (through voltage- or stretch-activated Na^+ channels and forward-mode of NCX) vs. active Na^+ influx (mainly through Na^+ - K^+ ATPase pump). The behaviour of these channels and transporters is difficult to predict and potentially complicated by the presence of neuronal isoforms of voltage-gated Na^+ channels (i.e. Nav1.1, Nav1.3 and Nav1.6) (Brette & Orchard, 2006; Maier et al., 2002; Maier et al., 2004; Vermij et al., 2020). Similar variations of vacuolated TT membrane resting potential can be predicted if K^+ fluxes are dysbalanced as a consequence

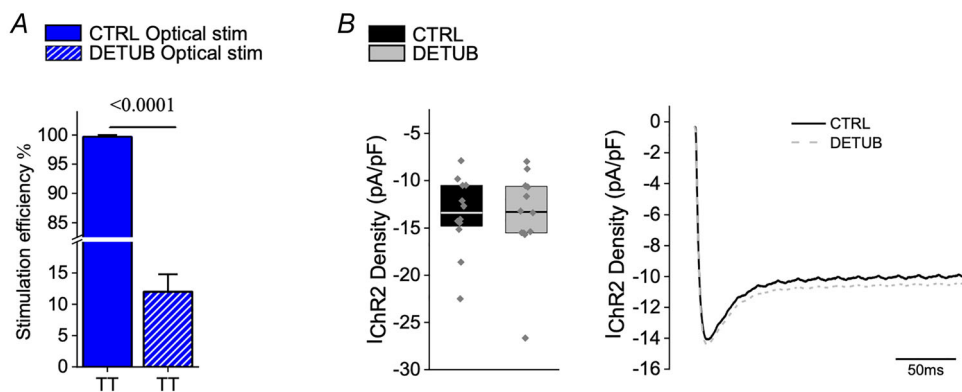


Figure 6. Loss of excitability of detached t-tubules

A, percentage of TT in which optical stimulation can trigger AP in CTRL and DETUB cells. Fisher's exact test was applied. B, average value and representative traces of IChR2 density provoked using 0.4 mW of light intensity from CTRL ($N = 3$, $n = 12$) and DETUB ($N = 3$, $n = 12$). Raw data are available at: <https://doi.org/10.6084/m9.figshare.23742231>. [Colour figure can be viewed at [wileyonlinelibrary.com](https://onlinelibrary.wiley.com)]

of K^+ accumulation in the TT lumen (with consequent depolarization of the K^+ equilibrium potential).

TT membrane excitability had previously been reported for skinned fibres of vertebrate skeletal muscle (Macdonald & Stephenson, 2004; Ortenblad & Stephenson, 2003; Pedersen et al., 2005; Posterino et al., 2000). In those experiments, the SS of muscle fibres was mechanically removed by rolling back the surface sarcolemma with forceps, forming a sort of 'cuff', whereas part of the TT system sealed off. In our report on isolated living cardiomyocytes, electrical uncoupling between SS and TT was achieved using transient osmotic shock that physically detaches TT membranes from the cell surface and, at the same time in principle, maintaining overall cell integrity, with intact SS and TT system components that are still operational and a near-native intracellular environment.

By contrast to skeletal muscle, cardiomyocyte activation *in vivo* occurs via electrotonic interaction with neighbouring cells, AP duration is longer (by one to two orders of magnitude, depending on species) and ECC involves trans-sarcolemmal calcium fluxes, making cells highly responsive to changes in local ion concentrations and regulatory influences on ion flux pathways. For these reasons, we consider that the osmotic shock-based approach is more appropriate for cardiomyocytes compared to membrane stripping.

Our study shows that TT do not merely represent a 'current sink' compartment that is driven by the SS 'source', but rather that TT are part of an overall excitable membrane system in which SS and TT affect each other. We are unable to assess whether this is a general feature that applies to the entire TT membrane

system. However, even if TT membrane excitability was non-uniform, any presence of excitable TT segments would affect AP conduction within the TT because such regions would act as repeater stations, reconditioning the AP signal amplitude. Several considerations regarding the physiological and patho-physiological consequences of TT excitability can be made.

The capacity of TT to generate AP may help to sustain spatio-temporal homogeneities of membrane depolarization within the TT network, which may be challenged when the TT system is structurally remodelled, such as in disease. In healthy cardiomyocytes, the characteristic length constant of electrotonic conduction along TT membranes is one order of magnitude larger than cell radius (Kong et al., 2018; Scardigli et al., 2017), although the utility of this length constant as a measure to predict spatial voltage uniformity within the TT network is questionable in supra-threshold voltage ranges (i.e. because membrane resistance markedly varies during the AP). The scenario becomes even more complex in atrial cardiomyocytes, where the transverse tubular system is less developed, whereas axial elements are more dominant (Brandenburg et al., 2016; Brandenburg et al., 2018; Richards et al., 2011). Furthermore, in healthy ventricular cardiomyocytes, no significant voltage gradient is expected, whereas, in a pathologically remodelled tubular system (Ibrahim et al., 2011), the resistance of the TT system may significantly increase and some tubular elements can be poorly coupled or even electrically uncoupled from the SS (Sacconi et al., 2012).

The pathophysiological relevance of TT excitability remains to be elucidated. Interestingly, behaviour similar

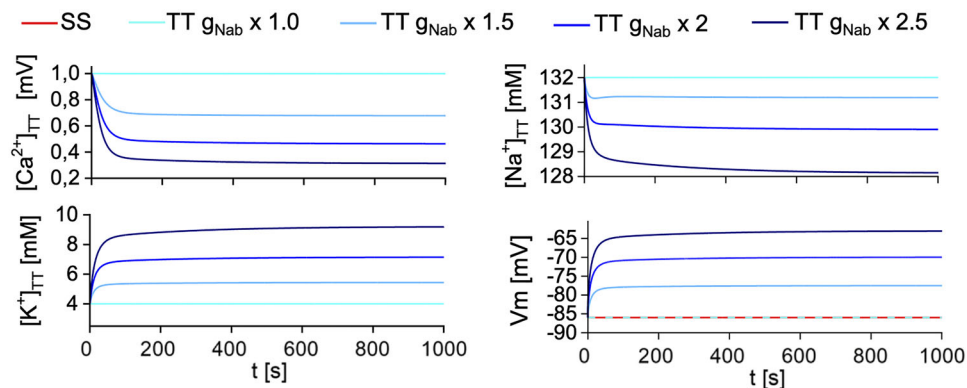


Figure 7. Changes of TT ion concentrations

Simulation of changes of TT concentrations and resting membrane voltage over time in detached TT in control conditions (cyan line) and when background Na^+ current (g_{Nab}) was increased by $1.5\times$ (light blue line), $2\times$ (blue line) and $2.5\times$ (dark blue line) at $[Na^+]_e = 132$ mM, $[K^+]_e = 4$ mM and $[Ca^{2+}]_e = 1$ mM. The model takes into account the experimentally used different levels of external ion concentrations during detubulation ($[Na^+]_e = 133$ mM, $[K^+]_e = 4.8$ mM and $[Ca^{2+}]_e = 0.5$ mM) and during the recordings ($[Na^+]_e = 132$ mM, $[K^+]_e = 4$ mM and $[Ca^{2+}]_e = 1$ mM). The transmembrane voltage at the SS is denoted by red line. Raw data are available at: <https://doi.org/10.6084/m9.figshare.23742231>. [Colour figure can be viewed at [wileyonlinelibrary.com](https://onlinelibrary.wiley.com)]

to that observed in the present study has been reported previously in pathological conditions (Crocini et al., 2014; Crocini et al., 2016) where, in electrically isolated TT, local supra-threshold voltage transients were observed. These spontaneous TT depolarizations may trigger large local SR Ca^{2+} releases (voltage-associated Ca^{2+} sparks, V-sparks) and potentially initiate arrhythmias. Future investigations will focus on exploring the relevance of TT excitability in cardiomyocytes for which ECC homogeneity has been challenged as a consequence of a pathologically remodelled TT system, employing the experimental approach described here to dissect TT and SS excitability and AP features. At present, however, we can unequivocally confirm that TT membranes in intact cardiomyocytes can be electrically excitable.

Appendix

A biophysically detailed computer model of a mouse ventricular cardiomyocyte, incorporating both surface

sarcolemma (SS) and t-tubular membrane (TT) was used (Fig. A1).

Geometric parameters of cell and of cellular compartments. The total volume of the model cell (V_C) was set to 10 pL. The fractional volumes of cytosolic space and dyadic space, as well as of network and junctional (release) compartments of the sarcoplasmic reticulum (NSR, JSR) are as in the original rat ventricular cardiomyocyte model (Pasek et al., 2006): 0.585, 75×10^{-6} , 0.0315 and 0.0035, respectively. The fractional volume of TT was set to 3.2% (Clark et al., 2001).

Membrane capacitance. According to our experimental data, the mean values of membrane capacitance (C) in intact (C_{CTRL}) and detubulated (C_{DETUB}) cells were 193 and 126 pF, respectively, and the mean fraction of TT resisting detubulation (TT_{res}) was 0.3. Assuming that the specific membrane capacitance is comparable in both membrane domains, the following equations allow

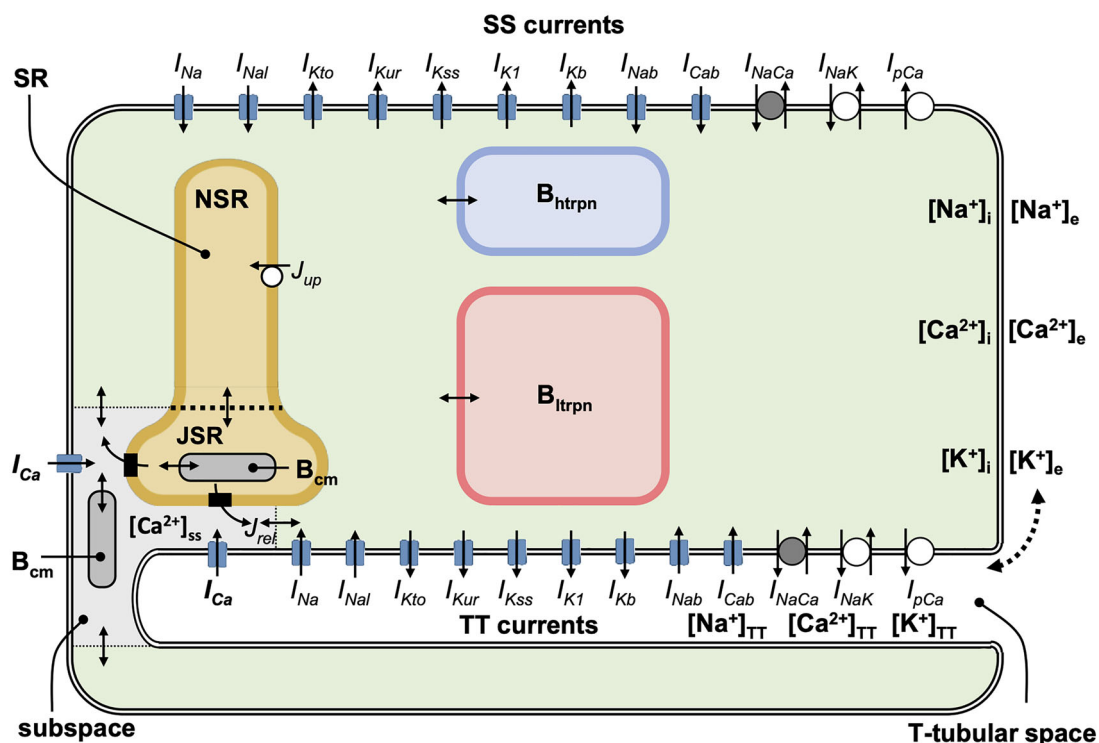


Figure A1. Schematic diagram of the mouse ventricular myocyte model

The description of electrical activity of SS and TT comprises the formulation of the following ion currents: fast Na^+ current (I_{Na}), late Na^+ current (I_{NaL}), L-type Ca^{2+} current (I_{Ca}), time-dependent transient outward K^+ current (I_{Kto}), ultrarapidly activating delayed rectifier K^+ current (I_{Kur}), non-inactivating steady-state K^+ current (I_{Kss}), time independent inward rectifier K^+ current (I_{K1}), background Na^+ current (I_{Nab}), background Ca^{2+} current (I_{Cab}), background K^+ current (I_{Kb}), Na^+ - Ca^{2+} exchange current (I_{NaCa}), Na^+ - K^+ ATPase pump current (I_{NaK}) and sarcolemmal Ca^{2+} pump current (I_{pCa}). The intracellular space contains the subspace, the network and junctional compartments of the sarcoplasmic reticulum (NSR, JSR) and the Ca^{2+} buffers calmodulin (B_{cm}), troponin (B_{htrpn} , B_{itprn}) and calsequestrin (B_{cs}). The small filled rectangles in JSR membrane represent ryanodine receptors. The small bi-directional arrows denote Ca^{2+} diffusion and the thick dashed arrow represents ionic diffusion between the TT and the external bulk spaces. [Colour figure can be viewed at wileyonlinelibrary.com]

calculation of the membrane capacitance in TT and SS (C_{TT} and C_{SS}):

$$C_{CTRL} = C_{SS} + C_{TT} \quad (1)$$

$$C_{DETUB} = C_{SS} + TT_{res} \cdot C_{TT} \quad (2)$$

$$C_{CTRL} = 193 \text{ pF}; C_{DETUB} = 126 \text{ pF};$$

$$TT_{res} = 0.3 \Rightarrow C_{SS} = 97.3 \text{ pF}; C_{TT} = 95.7 \text{ pF} \quad (3)$$

The conclusion that about half of the total sarcolemmal surface is in TT in mouse ventricular cardiomyocytes is consistent with a previous optical study by Forbes et al. (1984). Applying such data to a model with a total membrane area of $10,000 \mu\text{m}^2$ and a specific membrane capacitance of $1 \mu\text{F cm}^{-2}$, the modelled TT and SS have an identical capacitance of 50 pF.

Membrane currents. To simulate more closely the behaviour of mouse ventricular septal cardiomyocyte (Anumonwo et al., 2001), the following modifications of membrane transport systems were implemented.

- (i) The conductance of I_{Na} -channels (g_{Na}) was increased from 10 to 13.3 mS cm^{-2} to adjust the maximum upstroke velocity to $\sim 150 \text{ V s}^{-1}$ as observed experimentally (Anumonwo et al., 2001). Additionally, the membrane Na^+ transport was supplemented by a formulation of late Na^+ current (I_{NaL}), adopted from the mouse ventricular myocyte model of Morotti et al. (2014). The corresponding conductance (g_{NaL}) was set to $6.5 \mu\text{S cm}^{-2}$.
- (ii) The permeability of I_{Ca} -channels (P_{Ca}) was decreased from 2.1×10^{-4} to $0.7 \times 10^{-4} \text{ cm s}^{-1}$ and the time constant of voltage-dependent activation of I_{Ca} ($\tau_{Ca,VDA}$) was adjusted to reduce the rate of I_{Ca} deactivation in later phases of AP repolarization (negative to -20 mV), allowing the model AP duration at 75% repolarization to approach the value of $20.9 \pm 1.3 \text{ ms}$, measured in mouse ventricular cardiomyocytes at 1 Hz stimulation (Guo et al., 1999).
- (iii) The conductance of I_{Kto} -channels (g_{Kto}) was decreased from 0.35 to 0.146 mS cm^{-2} and gating characteristics of the channels were reformulated to mimic the parameters of early AP repolarization ($APD_{25} = 4 \pm 0.2 \text{ ms}$ and $APD_{50} = 8.5 \pm 0.3$), measured at 1 Hz (Guo et al., 1999).
- (iv) The formulations of I_{Ks} -channels (non-inactivating steady-state K^+ current) and of the newly added I_{Kur} -channels (ultra-rapid component of the delayed rectifier K^+ current) were adopted from the model of mouse ventricular myocytes developed by (Pandit, 2003) that is available in the CellML model repository (<https://models.cellml.org/cellml>).

Table A1. Electrical properties of ion transport systems in the model of mouse ventricular myocyte. Parameters of individual transporters (conductance (g), permeability (P), maximum current ($I_{XX,max}$) or scaling factor (k_{NaCa}))

Parameter	Value	f_x	Parameter	Value	f_x
g_{Na}	13.3 mS cm^{-2}	0.5	g_{Nab}	$1.2 \mu\text{S cm}^{-2}$	0.5
g_{NaL}	$6.5 \mu\text{S cm}^{-2}$	0.5	g_{Cab}	$0.367 \mu\text{S cm}^{-2}$	0.5
P_{Ca}	$0.7 \times 10^{-4} \text{ cm s}^{-1}$	0.87	g_{Kb}	$1.380 \mu\text{S cm}^{-2}$	0.5
g_{Kto}	0.146 mS cm^{-2}	0.5	k_{NaCa}	$0.18 \text{ nA cm}^{-2} \text{ mM}^{-4}$	0.5
g_{Kss}	0.075 mS cm^{-2}	0.5	$I_{NaK,max}$	$1.4 \mu\text{A cm}^{-2}$	0.5
g_{Kur}	0.085 mS cm^{-2}	0.5	$I_{pCa,max}$	$0.21 \mu\text{A cm}^{-2}$	0.5
g_{K1}	0.159 mS cm^{-2}	0.5			

$f_{x,t}$ represents the TT fraction of the ion transporter underlying current I_x .

The related conductances g_{Kss} and g_{Kur} were set to 0.075 and 0.085 mS cm^{-2} , respectively.

- (v) Other changes to the original rat model include: decrease of g_{K1} from 0.24 to 0.159 mS cm^{-2} , omission of hyperpolarization-activated current (I_f), increase of g_{Nab} (background Na^+ conductance) from 0.8 to $1.2 \mu\text{S cm}^{-2}$, decrease of g_{Cab} (background Ca^{2+} conductance) from 0.648 to $0.367 \mu\text{S cm}^{-2}$ (Anumonwo et al., 2001), increase of $I_{NaK,max}$ (maximal density of Na^+ - K^+ ATPase current) from 1 to $1.4 \mu\text{A cm}^{-2}$ and of Na^+ -half-saturation constant for I_{NaK} from 10 to 21 mM (Anumonwo et al., 2001), and decrease of $I_{pCa,max}$ (maximal density of sarcolemmal Ca^{2+} -pump current) from 0.85 to $0.21 \mu\text{A cm}^{-2}$ (summarized in Table A1).

Consistent with the absence of changes in I_{Na} , I_K , and membrane resting potential after detubulation as well as with excess of I_{Ca} at the TT membrane (Fig. 1), we simplified the distribution of ion transporters by setting all fractions to 0.5 (uniform distribution between the TT and SS membranes), with the exception of L-type Ca^{2+} current (f_{Ca}).

f_{Ca} was estimated on the basis of measurements of membrane capacitance and corresponding current densities in intact and detubulated cardiomyocytes (C_{CTRL} , C_{DETUB} , $I_{x,CTRL}$, $I_{x,DETUB}$) and relations derived in Pasek et al., 2017; Pasek et al., 2021):

$$I_{x,ratio} = \frac{I_{x,CTRL}C_{CTRL} - I_{x,DETUB}C_{DETUB}}{I_{x,CTRL}C_{CTRL}TT_{res} - I_{x,DETUB}C_{DETUB}}$$

$$\frac{C_{CTRL}TT_{res} - C_{DETUB}}{C_{CTRL} - C_{DETUB}} \quad (4)$$

$$f_x = \frac{I_{x,ratio}}{C_{SS}/C_{TT} + I_{x,ratio}} \quad (5)$$

where the $I_{x, \text{ratio}}$ represents the ratio between current densities in the TT and SS membranes ($I_{x, \text{TT}}/I_{x, \text{SS}}$), TT_{res} stands for the fraction of TT resisting detubulation, and C_{TT} and C_{SS} represent the membrane capacitance of the respective membrane domains. Assuming that $C_{\text{TT}} \approx C_{\text{SS}}$, and taking into account the mean values of C_{CTRL} and C_{DETUB} in a subpopulation of cells used for our I_{Ca} measurement ($C_{\text{CTRL}} = 162 \text{ pF}$, $C_{\text{DETUB}} = 97 \text{ pF}$), we conclude that the TT_{res} was ~ 0.2 in the corresponding cells (see

eqns 1 and 2). Using the mean values of $I_{\text{Ca}, \text{CTRL}}$ and $I_{\text{Ca}, \text{DETUB}}$ (6.5 and 3.26 pA/pF, respectively) and inserting these data into eqns 4 and 5 gives $I_{\text{Ca}, \text{ratio}}$ of 6.9 and f_{Ca} of 0.87, which corresponds well with the previous estimates done by Gadeberg et al. (2017b) suggesting predominant localization of I_{Ca} -channels in TT of mouse ventricular cardiomyocytes. The electrical properties of all ion transport systems used in the model are summarized in Table A1.

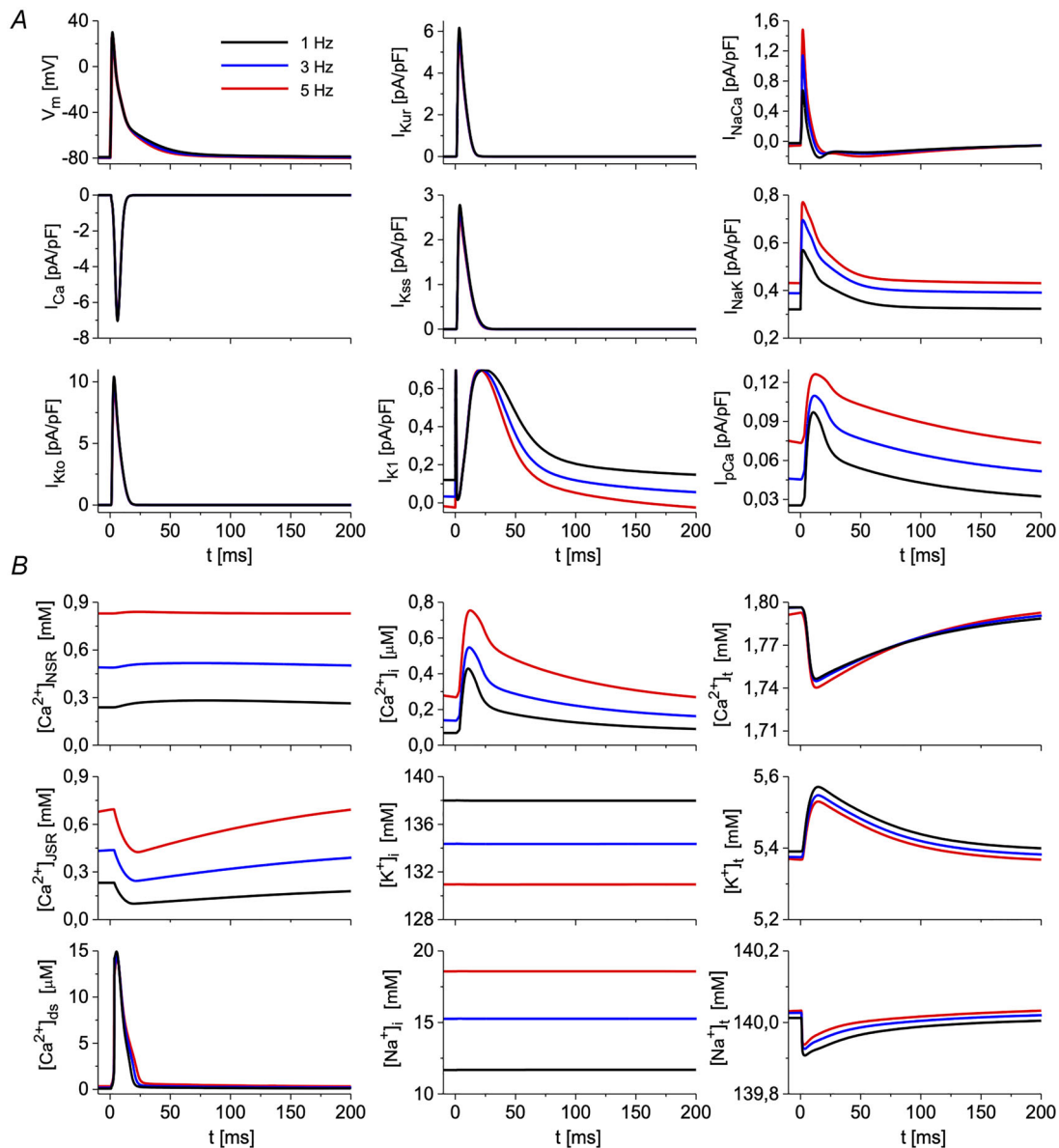


Figure A2. Behaviour of the model of a mouse ventricular cardiomyocyte at 1, 3 and 5 Hz steady-state stimulation

A, membrane voltage (V_m) and ion currents (I_{Na} , I_{Ca} , I_{Kto} , I_{Kur} , I_{Kss} , I_{K1} , I_{NaK} , I_{NaCa} , I_{pCa}). B, ion concentration changes in network and junctional (release) compartments of the SR ($[\text{Ca}^{2+}]_{\text{NSR}}$, $[\text{Ca}^{2+}]_{\text{JSR}}$), in dyadic space and bulk cytoplasm ($[\text{Ca}^{2+}]_{\text{ds}}$, $[\text{Ca}^{2+}]_{\text{i}}$, $[\text{K}^+]_{\text{i}}$, $[\text{Na}^+]_{\text{i}}$) and in TT ($[\text{Ca}^{2+}]_{\text{t}}$, $[\text{K}^+]_{\text{t}}$, $[\text{Na}^+]_{\text{t}}$). Extracellular ion concentrations were set to physiological values: $[\text{Na}^+]_{\text{e}} = 140 \text{ mM}$, $[\text{K}^+]_{\text{e}} = 5.4 \text{ mM}$ and $[\text{Ca}^{2+}]_{\text{e}} = 1.8 \text{ mM}$. [Colour figure can be viewed at wileyonlinelibrary.com]

Intracellular Ca^{2+} - handling. To simulate the increase of the systolic and diastolic maxima of intracellular Ca^{2+} transients with stimulation frequency observed in mouse ventricular cardiomyocytes by Ito et al. (2000), the forward rate parameter of SR Ca^{2+} ATPase was decreased from 0.4 to 0.2 mM s^{-1} and the slope factor controlling the $[\text{Na}^+]_i$ dependence of Na^+/K^+ pump was increased from 1.5 to 2.15.

Rate of ion exchange between TT and external space. The time constant of K^+ exchange between the TT and external space ($\tau_{\text{K,te}}$) was set to 50 ms to comply with the average rate of tail current decay observed at the end of depolarizing steps from -80 mV to the voltages between -30 and 40 mV (Clark et al., 2001). $\tau_{\text{Na,te}}$ was set to the same value as $\tau_{\text{K,te}}$ and $\tau_{\text{Ca,te}}$ was set to 167 ms to respect the ratio $\tau_{\text{Ca,te}}/\tau_{\text{K,te}}$ in the original rat model (Pasek et al., 2006).

Basic behaviour of the model. The basic behaviour of the mouse ventricular cell model is illustrated in Fig. A2. It shows superimposed action potential (AP) shapes, principal membrane currents, and ion concentrations in intracellular and extracellular compartments during 1, 3 and 5 Hz steady-state stimulation (after 600 s of stabilization). Similarly to the model by Bondarenko et al. (2004), the characteristics of AP reproduced by our model ($\text{APD}_{25} = 4$ ms, $\text{APD}_{50} = 8$ ms and $\text{APD}_{75} = 16$ ms at 1 Hz) agree well with experimentally measured values (Guo et al., 1999) and change only slightly with stimulation frequency (Guo et al., 2000). The model reconstruction of experimental data of Ito et al. (2000), showing a frequency-dependent increase in the systolic and diastolic maxima of intracellular Ca^{2+} transients, is illustrated in Fig. A3.

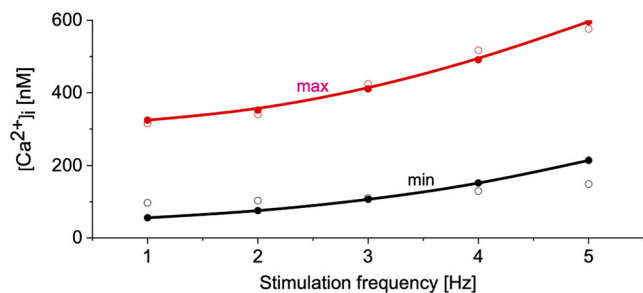


Figure A3. Model reconstruction of the frequency dependence of intracellular Ca^{2+} transient amplitudes in mouse ventricular myocytes

Black and red empty circles represent minimal (diastolic) and maximal (systolic) values of Ca^{2+} transients in experiments (Ito et al. 2000), respectively. Black and red full circles represent corresponding data from the model. Extracellular ion concentrations in experiment and model: $[\text{Na}^+]_e = 137$ mM, $[\text{K}^+]_e = 3.7$ mM and $[\text{Ca}^{2+}]_e = 1.5$ mM. [Colour figure can be viewed at wileyonlinelibrary.com]

References

- Anumonwo, J. M. B., Tallini, Y. N., Vetter, F. J., & Jalife, J. (2001). Action potential characteristics and arrhythmogenic properties of the cardiac conduction system of the murine heart. *Circulation Research*, **89**(4), 329–335.
- Berry, R., Despa, S., Fuller, W., Bers, D., & Shattock, M. (2007). Differential distribution and regulation of mouse cardiac Na^+/K^+ -ATPase alpha1 and alpha2 subunits in T-tubule and surface sarcolemmal membranes. *Cardiovascular Research*, **73**(1), 92–100.
- Bers, D. M. (2002). Cardiac excitation-contraction coupling. *Nature*, **415**(6868), 198–205.
- Bondarenko, V. E., Szigeti, G. P., Bett, G. C. L., Kim, S.-J., & Rasmusson, R. L. (2004). Computer model of action potential of mouse ventricular myocytes. *American Journal of Physiology-Heart and Circulatory Physiology*, **287**(3), H1378–H1403.
- Bossuyt, J., Despa, S., Han, F., Hou, Z., Robia, S. L., Lingrel, J. B., & Bers, D. M. (2009). Isoform specificity of the Na/K -ATPase association and regulation by phospholemman. *The Journal of Biological Chemistry*, **284**(39), 26749–26757.
- Brandenburg, S., Kohl, T., Williams, G. S. B., Gusev, K., Wagner, E., Rog-Zielinska, E. A., Hebisch, E., Dura, M., Didié, M., Gotthardt, M., Nikolaev, V. O., Hasenfuss, G., Kohl, P., Ward, C. W., Lederer, W. J., & Lehnart, S. E. (2016). Axial tubule junctions control rapid calcium signaling in atria. *The Journal of Clinical Investigation*, **126**(10), 3999–4015.
- Brandenburg, S., Pawlowitz, J., Fakuade, F. E., Kownatzki-Danger, D., Kohl, T., Mitronova, G. Y., Scardigli, M., Neef, J., Schmidt, C., Wiedmann, F., Pavone, F. S., Sacconi, L., Kutschka, I., Sossalla, S., Moser, T., Voigt, N., & Lehnart, S. E. (2018). Axial tubule junctions activate atrial $\text{Ca}(2+)$ release across species. *Frontiers in Physiology*, **9**, 1227.
- Brette, F., & Orchard, C. H. (2006). No apparent requirement for neuronal sodium channels in excitation-contraction coupling in rat ventricular myocytes. *Circulation Research*, **98**(5), 667–674.
- Bruegmann, T., Malan, D., Hesse, M., Beiert, T., Fuegeman, C. J., Fleischmann, B. K., & Sasse, P. (2010). Optogenetic control of heart muscle in vitro and in vivo. *Nature Methods*, **7**(11), 897–900.
- Clark, R. B., Tremblay, A., Melnyk, P., Allen, B. G., Giles, W. R., & Fiset, C. (2001). T-tubule localization of the inward-rectifier $\text{K}(+)$ channel in mouse ventricular myocytes: A role in $\text{K}(+)$ accumulation. *The Journal of Physiology*, **537**(3), 979–992.
- Crocini, C., Coppini, R., Ferrantini, C., Yan, P., Loew, L. M., Tesi, C., Cerbai, E., Poggesi, C., Pavone, F. S., & Sacconi, L. (2014). Defects in T-tubular electrical activity underlie local alterations of calcium release in heart failure. *Proceedings of the National Academy of Sciences*, **111**(42), 15196–15201.

- Crocini, C., Ferrantini, C., Scardigli, M., Coppini, R., Mazzoni, L., Lazzeri, E., Pioner, J. M., Scellini, B., Guo, A., Song, L. S., Yan, P., Loew, L. M., Tardiff, J., Tesi, C., Vanzi, F., Cerbai, E., Pavone, F. S., Sacconi, L., & Poggesi, C. (2016). Novel insights on the relationship between T-tubular defects and contractile dysfunction in a mouse model of hypertrophic cardiomyopathy. *Journal of Molecular and Cellular Cardiology*, **91**, 42–51.
- Despa, S., & Bers, D. M. (2007). Functional analysis of Na^+/K^+ -ATPase isoform distribution in rat ventricular myocytes. *American Journal of Physiology-Cell Physiology*, **293**(1), C321–C327.
- Drobizhev, M., Makarov, N. S., Tillo, S. E., Hughes, T. E., & Rebane, A. (2011). Two-photon absorption properties of fluorescent proteins. *Nature Methods*, **8**(5), 393–399.
- Ferrantini, C., Coppini, R., Sacconi, L., Tosi, B., Zhang, M. L., Wang, G. L., De Vries, E., Hoppenbrouwers, E., Pavone, F., Cerbai, E., Tesi, C., Poggesi, C., & Ter Keurs, H. E. D. J. (2014). Impact of detubulation on force and kinetics of cardiac muscle contraction. *Journal of General Physiology*, **143**(6), 783–797.
- Forbes, M. S., Hawkey, L. A., & Sperelakis, N. (1984). The transverse-axial tubular system (TATS) of mouse myocardium: Its morphology in the developing and adult animal. *American Journal of Anatomy*, **170**(2), 143–162.
- Franzini-Armstrong, C., Venosa, R. A., & Horowicz, P. (1973). Morphology and accessibility of the 'transverse' tubular system in frog sartorius muscle after glycerol treatment. *The Journal of Membrane Biology*, **14**(1), 197–212.
- Gadeberg, H. C., Kong, C. H. T., Bryant, S. M., James, A. F., & Orchard, C. H. (2017a). Sarcolemmal distribution of $\text{I}(\text{Ca})$ and $\text{I}(\text{NCX})$ and $\text{Ca}(2+)$ autoregulation in mouse ventricular myocytes. *American Journal of Physiology-Heart and Circulatory Physiology*, **313**(1), H190–H199.
- Gadeberg, H. C., Kong, C. H. T., Bryant, S. M., James, A. F., & Orchard, C. H. (2017b). Sarcolemmal distribution of $\text{I}(\text{Ca})$ and $\text{I}(\text{NCX})$ and $\text{Ca}(2+)$ autoregulation in mouse ventricular myocytes. *American Journal of Physiology-Heart and Circulatory Physiology*, **313**(1), H190–H199.
- Guo, A., & Song, L.-S. (2014). AutoTT: Automated detection and analysis of T-tubule architecture in cardiomyocytes. *Biophysical Journal*, **106**(12), 2729–2736.
- Guo, W., Li, H., London, B., & Nerbonne, J. M. (2000). Functional consequences of elimination of $\text{i}(\text{to},\text{f})$ and $\text{i}(\text{to},\text{s})$: Early afterdepolarizations, atrioventricular block, and ventricular arrhythmias in mice lacking $\text{Kv}1.4$ and expressing a dominant-negative $\text{Kv}4$ alpha subunit. *Circulation Research*, **87**(1), 73–79.
- Guo, W., Xu, H., London, B., & Nerbonne, J. M. (1999). Molecular basis of transient outward K^+ current diversity in mouse ventricular myocytes. *The Journal of Physiology*, **521**(Pt 3), 587–599.
- Hochbaum, D. R., Zhao, Y., Farhi, S. L., Klapoetke, N., Werley, C. A., Kapoor, V., Zou, P., Kralj, J. M., Maclaurin, D., Smedemark-Margulies, N., Saulnier, J. L., Boulting, G. L., Straub, C., Cho, Y. K., Melkonian, M., Wong, G. K. A.-S., Harrison, D. J., Murthy, V. N., Sabatini, B. L., Boyden, E. S., Campbell, R. E., & Cohen, A. E. (2014). All-optical electrophysiology in mammalian neurons using engineered microbial rhodopsins. *Nature Methods*, **11**(8), 825–833.
- Ibrahim, M., Gorelik, J., Yacoub, M. H., & Terracciano, C. M. (2011). The structure and function of cardiac t-tubules in health and disease. *Proceedings Biological Sciences*, **278**, 2714–2723.
- Ito, K., Yan, X., Tajima, M., Su, Z., Barry, W. H., & Lorell, B. H. (2000). Contractile reserve and intracellular calcium regulation in mouse myocytes from normal and hypertrophied failing hearts. *Circulation Research*, **87**(7), 588–595.
- Kawai, M., Hussain, M., & Orchard, C. H. (1999). Excitation-contraction coupling in rat ventricular myocytes after formamide-induced detubulation. *The American Journal of Physiology*, **277**, H603–609.
- Kong, C. H. T., Rog-Zielinska, E. A., Kohl, P., Orchard, C. H., & Cannell, M. B. (2018). Solute movement in the t-tubule system of rabbit and mouse cardiomyocytes. *Proceedings of the National Academy of Sciences*, **115**(30), E7073–E7080.
- Macdonald, W. A., & Stephenson, D. G. (2004). Effects of ADP on action potential-induced force responses in mechanically skinned rat fast-twitch fibres. *The Journal of Physiology*, **559**(2), 433–447.
- Maier, S. K. G., Westenbroek, R. E., McCormick, K. A., Curtis, R., Scheuer, T., & Catterall, W. A. (2004). Distinct subcellular localization of different sodium channel alpha and beta subunits in single ventricular myocytes from mouse heart. *Circulation*, **109**(11), 1421–1427.
- Maier, S. K. G., Westenbroek, R. E., Schenkman, K. A., Feigl, E. O., Scheuer, T., & Catterall, W. A. (2002). An unexpected role for brain-type sodium channels in coupling of cell surface depolarization to contraction in the heart. *Proceedings of the National Academy of Sciences of the United States of America*, **99**(6), 4073–4078.
- Moench, I., & Lopatin, A. N. (2014). $\text{Ca}(2+)$ homeostasis in sealed t-tubules of mouse ventricular myocytes. *Journal of Molecular and Cellular Cardiology*, **72**, 374–383.
- Morotti, S., Edwards, A. G., McCulloch, A. D., Bers, D. M., & Grandi, E. (2014). A novel computational model of mouse myocyte electrophysiology to assess the synergy between Na^+ loading and CaMKII . *The Journal of Physiology*, **592**(6), 1181–1197.
- Nyns, E. C. A., Kip, A., Bart, C. I., Plomp, J. J., Zeppenfeld, K., Schalij, M. J., de Vries, A. A. F., & Pijnappels, D. A. (2017). Optogenetic termination of ventricular arrhythmias in the whole heart: Towards biological cardiac rhythm management. *European Heart Journal*, **38**, 2132–2136.
- Ortenblad, N., & Stephenson, D. G. (2003). A novel signalling pathway originating in mitochondria modulates rat skeletal muscle membrane excitability. *The Journal of Physiology*, **548**, 139–145.
- Pandit, S. V. (2003). Electrical Activity in Murine Ventricular Myocytes: Simulation Studies. *Chapter 5: Ionic Basis of Cardiac Repolarization in Mouse: Quantitative Insights*.
- Pásek, M., Šimurda, J., Bébarová, M., & Christé, G. (2021). Divergent estimates of the ratio between Na^+ - Ca^{2+} current densities in t-tubular and surface membranes of rat ventricular cardiomyocytes. *Journal of Cell Science*, **134**(14), jcs258228.

- Pasek, M., Simurda, J., & Christe, G. (2006). The functional role of cardiac T-tubules explored in a model of rat ventricular myocytes. *Philosophical Transactions Series A, Mathematical, Physical, and Engineering Sciences*, **364**, 1187–1206.
- Pásek, M., Šimurda, J., & Christé, G. (2017). Different Densities of Na-Ca exchange current in T-Tubular and surface membranes and their impact on cellular activity in a model of rat ventricular cardiomyocyte. *BioMed Research International*, **2017**, 6343821.
- Pedersen, T. H., De Paoli, F., & Nielsen, O. B. (2005). Increased excitability of acidified skeletal muscle: Role of chloride conductance. *Journal of General Physiology*, **125**(2), 237–246.
- Posterino, G. S., Lamb, G. D., & Stephenson, D. G. (2000). Twitch and tetanic force responses and longitudinal propagation of action potentials in skinned skeletal muscle fibres of the rat. *The Journal of Physiology*, **527**(Pt 1), 131–137.
- Pulicherla, N., Shen, S., Yadav, S., Debbink, K., Govindasamy, L., Agbandje-Mckenna, M., & Asokan, A. (2011). Engineering liver-detargeted AAV9 vectors for cardiac and musculoskeletal gene transfer. *Molecular Therapy*, **19**(6), 1070–1078.
- Richards, M. A., Clarke, J. D., Saravanan, P., Voigt, N., Dobrev, D., Eisner, D. A., Trafford, A. W., & Dibb, K. M. (2011). Transverse tubules are a common feature in large mammalian atrial myocytes including human. *American Journal of Physiology-Heart and Circulatory Physiology*, **301**(5), H1996–H2005.
- Sacconi, L., Ferrantini, C., Lotti, J., Coppini, R., Yan, P., Loew, L. M., Tesi, C., Cerbai, E., Poggesi, C., & Pavone, F. S. (2012). Action potential propagation in transverse-axial tubular system is impaired in heart failure. *Proceedings of the National Academy of Sciences*, **109**(15), 5815–5819.
- Scardigli, M., Crocini, C., Ferrantini, C., Gabbriellini, T., Silvestri, L., Coppini, R., Tesi, C., Rog-Zielinska, E. A., Kohl, P., Cerbai, E., Poggesi, C., Pavone, F. S., & Sacconi, L. (2017). Quantitative assessment of passive electrical properties of the cardiac T-tubular system by FRAP microscopy. *Proceedings of the National Academy of Sciences*, **114**(22), 5737–5742.
- Swift, F., Tovsrud, N., Enger, U., Sjaastad, I., & Sejersted, O. (2007). The Na⁺/K⁺-ATPase alpha2-isoform regulates cardiac contractility in rat cardiomyocytes. *Cardiovascular Research*, **75**(1), 109–117.
- Thomas, M. (2003). Localization and function of the Na⁺/Ca²⁺-exchanger in normal and detubulated rat cardiomyocytes. *Journal of Molecular and Cellular Cardiology*, **35**(11), 1325–1337.
- Tidball, J. G., Cederdahl, J. E., & Bers, D. M. (1991). Quantitative analysis of regional variability in the distribution of transverse tubules in rabbit myocardium. *Cell and Tissue Research*, **264**(2), 293–298.
- Vermij, S. H., Abriel, H., & Kucera, J. P. (2020). A fundamental evaluation of the electrical properties and function of cardiac transverse tubules. *Biochimica et biophysica acta Molecular Cell Research*, **1867**(3), 118502.
- Yan, P., Acker, C. D., Zhou, W.-L., Lee, P., Bollensdorff, C., Negrean, A., Lotti, J., Sacconi, L., Antic, S. D., Kohl, P., Mansvelder, H. D., Pavone, F. S., & Loew, L. M. (2012). Palette of fluorinated voltage-sensitive hemicyanine dyes. *Proceedings of the National Academy of Sciences of the United States of America*, **109**(50), 20443–20448.
- Zaglia, T., Pianca, N., Borile, G., Da Broi, F., Richter, C., Campione, M., Lehnart, S. E., Luther, S., Corrado, D., Miquerol, L., & Mongillo, M. (2015). Optogenetic determination of the myocardial requirements for extrasystoles by cell type-specific targeting of ChannelRhodopsin-2. *Proceedings of the National Academy of Sciences of the United States of America*, **112**, E4495–4504.

Additional information

Data availability statement

All data generated and analysed during this study are available on figshare (<https://doi.org/10.6084/m9.figshare.23742231>).

Competing interests

LML is a founder and owner of Potentiometric Probes, LLC, which holds an exclusive license for di-4-AN(F)EPPTA (trade name ElectroFluor630) from the University of Connecticut.

Author contributions

All authors have approved the final version of the manuscript and agree to be accountable for all aspects of the work. All persons designated as authors qualify for authorship, and all those who qualify for authorship are listed.

Funding

German Research Foundation: Peter Kohl, Leonardo Sacconi, DFG #422 681 845.

Acknowledgements

This work was supported by the European Union's Horizon 2020 research and innovation program under grant agreement no. 871124 Laserlab-Europe. P. Kohl and L. Sacconi are members of the German Research Foundation's Collaborative Research Centre SFB1425 (DFG #422681845). The work of M. Pásek was carried out with the Institutional Support RVO: 61388998.

Open access funding enabled and organized by Projekt DEAL.

Keywords

cardiac electrophysiology, excitation–contraction coupling, imaging

Supporting information

Additional supporting information can be found online in the Supporting Information section at the end of the HTML view of the article. Supporting information files available:

Peer Review History